Proceedings of the 9th International Conference on Cyclotrons and their Applications
September 1981, Caen, France

PRESENT STATUS OF HIRFL

Accelerator design group
(Presented By B. W. Wei)

Institute of Modern Physics, P.O.Box 31, Lanzhou, China

Abstract-. General features of the tandem cyclotron system are briefly reviewed. The revised time schedule of construction is reported. Recent experimental work on various systems of the main cyclotron is illustrated by somewhat detailed work on the magnet system.

The heavy ion research facility of Lanzhou (HIRFL) is a tandem cyclotron system. The main accelerator is a four 52° separated sector cyclotron (SSC) with the energy constant K=450, and the injector is a 1.7m sector focusing cyclotron (SFC) with K=69, which is to be converted from the existing 1.5m classical cyclotron. With this facility, we expect to accelerate light ions to a maximum energy of about 100 Mev/A and Xe ions to about 4.8 Mev/A, the beam intensity ranging from 10^{12} to 10^{10} P.P.S. respectively. Schematic diagram of the main accelerator and injector are shown in fig. 1-2, and the general layout of system in fig. 3. Some typical operating parameters, the main characteristics, the matching parameters between SFC and SSC, and the precisions and tolerances required for the sector magnet and rf system are given separately in tables 1-4.

A fairly detailed description of the main accelerator SSC and that of the injector SFC have been published elsewhere [1]. The main features of SSC are quite similar to that of GANIL[2]. The design of the facility was accomplished by the end of last year. But the calculation of the beam profile and phase diagrams through the injection and extraction systems and the beam transport system is now being checked in GANIL by using their programmes*. Preliminary results obtained show that some minor alternations will be needed for the beam transport system immediately after SFC and before SSC. Two more quadrupole doublets have to be added between SFC and the first 70° bending magnet in order to form a non-despersive image waisted both horizontally and vertically at the stripper to reduce the beam loss. The last quadrupole doublet before SSC will be moved forward about 1.2m in order to have more room for installing some beam diagnosis components. As for the injection and extraction systems, all the bending magnets are fixed but the positions of the electrostatic deflectors and the extraction magnetic channels should be made adjustable within a distance of about 5-20mm for ions from C^{6+} to Xe^{23+}.

Arrangement has been made for Chinese factories to build the main parts of the mechanical components and some power supplies of the accelerators. The design of the facility started at the end of 1976. The time schedule of construction is roughly as follows:

1) We shall have our first sector magnet next year. The sector magnet is made of forged low carbon steel. The metallurgical process was done in an alkaline open health furnace and casted in a vacuum tank with argon gas flowing through the tank to guarantee the homogeneity of the chemical compositions. The stabilized power supply ($\Delta I/I < 5X10^{-6}$) for this sector has been built in our laboratory and is now ready for use. That means, as soon as the first sector arrives at Lanzhou, it will be mounted properly and the work of field mapping immediately begin. If the results of measurement prove satisfactory, the remaining three magnet sectors will arrive one by one at intervals of about six months and therefore, we shall have the whole magnet system ready for the complete field measurement at the end of 1984 at latest.

2) The first rf cavity is scheduled to arrive in 1983. The generators are being

* I would like to take this opportunity to thank Dr. J.Ferme and Dr. R.Beck for their generous help in doing this work on behalf of my colleagues Mm. He and Wang.

manufactured in Shanghai. We expect that at least one of them will be available for testing the cavity before the latter arrives. A dummy vacuum system will be built for this purpose.

3) The design of the monolithic structure of the vacuum chamber follows almost exactly that of GANIL. But due to the difficulty of transportation it will be divided into four main parts machined separately in the factory, transported to Lanzhou and then welded together on site. The manufacturers who are well experienced in doing the stainless steel welding, have guaranteed the accuracy required by the design. In order to make sure of that, the welding of the vacuum chamber is scheduled to be done not later than 1984, so that enough time will be left to do the final machining after welding, if necessary.

4) Most of the smaller mechanical components such as bending magnets, magnetic lenses, beam line tubes, etc. will be manufactured in our own workshop. The prototypes of most of the stabilized D.C.power supplies have been built in our laboratory, and then passed to an electric factory for production if more than one is required.

5) The injector SFC will be ready for use before 1986. The study of PIG type heavy ion sources is now under way.

6) Lastly, we plan to have everything ready for assembling and final testing for the main accelerator in the winter of 1985 and hope to get our first beam in 1987.

In the mean while, the following experimental studies have been done or are still going on mostly in our laboratory and some jointly with other institution or Chinese factories: 1) the properties of the construction materials for the vacuum system, 2) the components of the beam diagnosis system and the control system, 3) electronic circuits for the stabilization of frequency, amplitude and phase of the rf system, 4) the properties of the bending magnets, magnetic channels and electrostatic deflectors, and 5) the computerized hall probe system for mapping and trimming the magnetic field of SSC. I should like to describe the last topic somewhat in detail for the rest of my talk.

A computer controlled system for mapping and trimming the magnetic field of the 1/4 scale model magnets has been built, including the Hall probe, the positioning device,a Solartron 7075 digital voltmeter for reading the Hall tension and a controlling computer. Siemens FC-32 Hall probe is stabilized at a temperature of (35± 0.1) ^{o}C and the Hall current at 70.29mA with a stability better than $5X10^{-5}$/8hrs. The positioning device is of polar type. The rotating arm can be turned azimuthally in steps of one degree within an angular range of 90^{o} and the radial position of the Hall probe moved along the arm in the range from r=56mm to 875mm in steps of 21.5mm. Both the azimuthal and radial positions of the probe are recorded automatically by the computer in coordination with the field mapping measurements. After the mapping of a certain field distribution has been done, if better trimming of the field is required, the computer is programmed to compare this distribution with the required one, say the isochronous field distribution of a certain type of heavy ions, and to calculate the corrections to the currents of the trimming coils by the least square method. Adjustments are then made manually to set the trimming currents to the corrected values according to the corrections thus obtained. This process is then repeated to optimize the trimming currents. If the initial values for the trimming currents have been chosen correctly, three or four iterations are enough for optimizing their values. An accuracy better than 0.1% can be obtained for the final field distribution compared with the required one.

1) Experiments of magnetic field mapping.- The following series of experiments was done in order to check how the automatic measuring system worked: a) mapping the magnetic field of a single ¼ scale model magnet (fig.4),b) mapping the magnetic field of two perpendicular-oriented sector magnets covering two hills and one valley (fig.5), and c) mapping the magnetic field of the same pair of the sector magnets but with curved shims for the edges of the sector poles (fig.6), designed for accelerating heavy ions at Bgap=16KG with the relativitic factor γ =1.05 at the radius of extraction. Some interesting results obtained directly from the system are illustrated in the following figures: a) the magnetic field along the median line of the hill excited in turn by 4 different magnetizing currents (fig.7),b) the azimuthal variation of magnetic field at the radius of 49.1cm (fig.8),c) the change of the magnetic angle of the sector magnet with B at three different radii compared with the geometrical angle (fig.9),d) the magnetic field along the median line of the valley between the two perpendicularly oriented sector magnets when one or both magnets were excited at Bgap=16KG (fig.10),e) the magnetic field averaged over a circular path between the median lines of the hill and the valley as a function of the radius when one or both magnets were excited at Bgap=16KG (fig.11),f) the magnetic field averaged over a circular path between the median lines of the hill and valley as a function of the radius for the curved edge sector magnets (fig.12), and g) the ratio $K(R)=B(0^{o},R)/\bar{B}_{G}(R)$ as a function of the radius (fig.13), where $\bar{B}_{G}$ is the magnetic field averaged over a Gordon path between the median lines of the hill and the valley and $B(0^{o},R)$ is the magnetic field along the median line of the hill. Fig.13 shows that the ratio K is essentially constant within the radial range from 25 to 75cm. That means, we probably could obtain the isochronous field distribution by trimming the magnetic field $B(0^{o},R)$ along the median line of the hill only assuming that

$\bar{B}_G = B(0^o,R)/\bar{K}$, where $\bar{K}$ is the average value of K(R).

2) Trimming of magnetic field and acquisition of the isochronous field.--As an empirical basis for trimming the magnetic field, the contribution to the field distribution for each single trimming coil excited with various excitation currents was carefully studied. Fig.14 and fig.15 illustrate some results of this work. They are quite similar to those of IUCF[3]. The experiments of trimming the magnetic field were then done by the least square method described above. Fig.16 illustrates the trimmed magnetic field B (0°, R) as the trimming coils were energized successively one by one with the currents indicated at the left corner of the figure. The final field distribution (the heavy curve 10+11) obtained is the isochronous field for accelerating C^{6+} to an energy of 50Mev/A. Fig.17 illustrates the magnetic field B(0°,R) for two successive least square adjustments of the trimming currents given in the table at the top of the figure for accelerating U^{36+} to an energy of 10Mev/A. Fig.18 illustrates the trimmed magnetic field $\bar{B}_G$ (R) for the curved edge sector case, averaged over the Gordon orbit for accelerating C^{6+} to an energy of 50Mev/A. Comparing fig.18 with fig.16, one can easily see the advantage of the curved edge sector over the straight one, that the trimming currents are much smaller and the precision higher for the former case. The phase history of accelerating C^{6+} with this field distribution has thereby been calculated and is illustrated in fig. 19.

The above series of experiments seems to prove that this automatic system worked quite satisfactorily. A similar system with 98 Hall probes for measuring and controlling the magnetic field of the full scale sector magnet has been designed and is to be built soon. The positioning device for the same is now under machining and will be completed next year.

I would like to take this opportunity on behalf of our accelerator design group to thank GANIL physicists and engineers for their help and collaboration in designing this facility since 1978. Some of us would like to thank for the hospitality of GANIL staff and the financial support granted by CEA and CNRS during their stay in Caen,

References

1) HIRFL group, proc. Japan-China joint symposium on accelerators for nuclear science and their applications, Atami, 8-11 sept. 1980
P63 and P390

2) J.Ferme, status report on GANIL, IEEE trans., NS-26, NO 2, april 1979.

3) D.L.Friesel and P.E.Pollock, IEEE trans., NS-22, No3 (1975) 1891

No.	beam	Z1	Z1/A	frev.1 MHZ	fr.f.1 MHZ	h1	$\bar{B}$ex KG	E1 Mev/A	(ΔE/E)1	ε πmmmrad	$\Delta\phi_i$	I1 P.P.S.
1	12C	2+	0.17	2.88	8.64	3	11.33	0.96	$\pm 1.2X10^{-3}$	15	6°	$7.8X10^{13}$
2	12C	4+	0.33	6.23	6.23	1	12.33	4.53	$\pm 1.2X10^{-3}$	15	6°	$1.9X10^{13}$
3	12C	5+	0.42	8.50	8.50	1	13.50	8.48	$\pm 1.2X10^{-3}$	15	6°	$1.3X10^{13}$
4	14N	5+	0.33	8.50	8.50	1	15.75	8.48	$\pm 1.2X10^{-3}$	15	6°	$6.3X10^{12}$
5	16O	6+	0.38	8.50	8.50	1	15.00	8.48	$\pm 1.2X10^{-3}$	15	6°	$6.3X10^{12}$
6	20Ne	8+	0.40	8.50	8.50	1	14.06	8.48	$\pm 1.2X10^{-3}$	15	6°	$4.7X10^{12}$
7	40Ar	10+	0.25	6.00	18.00	3	15.80	4.19	$\pm 2.8X10^{-3}$	15	10°	$2.2X10^{12}$
8	84Kr	10+	0.12	2.88	8.64	3	15.86	0.96	$\pm 1.2X10^{-3}$	15	6°	$6.3X10^{10}$
9	132Xe	11+	0.08	2.00	6.00	3	15.75	0.46	$\pm 1.2X10^{-3}$	15	6°	$7.8X10^{10}$
10	12C	3+	0.25	4.41	13.23	3	11.59	2.26	$\pm 2.8X10^{-3}$	15	10°	$5.2X10^{13}$
11	40Ar	4+	0.10	2.31	6.93	3	15.14	0.62	$\pm 1.2X10^{-3}$	15	6°	$2.3X10^{13}$
12	84Kr	7+	0.08	1.87	9.35	5	14.74	0.41	$\pm 1.2X10^{-3}$	15	6°	$1.7X10^{13}$

Table 1 a) Some typical operating parameters of SFC

NO.	beam	Z	Z/A	frev MHZ	frf MHZ	h	Bex KG	E Mev/A	$\Delta E/E$	ε πmmmrad	$\Delta\Phi$	I P.P.S.
1	12C	5+	0.42	2.16	8.64	4	5.67	10.0	$\pm 1.2X10^{-3}$	10	6°	$2.9X10^{13}$
2	12C	6+	0.50	4.68	9.36	2	10.78	50.0	$\pm 2.3X10^{-3}$	10	9°	$2.3X10^{12}$
3	12C	6+	0.50	6.38	12.76	2	15.44	100.0	$\pm 2.3X10^{-3}$	10	9°	$3.9X10^{11}$
4	14N	7+	0.50	6.38	12.76	2	15.44	100.0	$\pm 2.3X10^{-3}$	10	9°	$3.2X10^{11}$
5	16O	8+	0.50	6.38	12.76	2	15.44	100.0	$\pm 2.3X10^{-3}$	10	9°	$3.8X10^{11}$
6	20Ne	10+	0.50	6.38	12.76	2	15.44	100.0	$\pm 2.3X10^{-3}$	10	9°	$4.2X10^{11}$
7	40Ar	16+	0.40	4.50	9.00	2	12.91	46.0	$\pm 1.0X10^{-3}$	10	5°	$2.4X10^{11}$
8	84Kr	22+	0.26	2.16	8.64	4	9.11	10.0	$\pm 1.2X10^{-3}$	10	6°	$1.9X10^{10}$
9	132Xe	23+	0.17	1.50	9.00	6	9.47	4.8	$\pm 2.3X10^{-3}$	10	9°	$9.1X10^{9}$
10	12C	6+	0.50	3.30	13.20	4	7.42	24.0	$\pm 1.0X10^{-3}$	10	5°	$9.8X10^{12}$
11	40Ar	11+	0.28	1.73	13.84	8	6.93	6.4	$\pm 2.3X10^{-3}$	10	9°	$5.5X10^{12}$
12	84Kr	17+	0.20	1.40	14.00	10	7.63	4.2	$\pm 2.3X10^{-3}$	10	9°	$3.1X10^{12}$
13	238U	36+	0.15	2.16	12.96	6	15.79	10.0				

Table 1b) Some typical operating parameters of SSC

Injection mean radius	1.00m	Exciting amp.turns	$1.7X10^{5}$ AW
Extraction mean radius	3.21m	Maximum radius of the pole face	358.4cm
Radial betatron frequency ν_R	1.087-1.202	Minimum radius of the pole face	84.0cm
Vertical betatron frequency ν_z	0.742-0.864	Sector width	330cm
Energy gain	10.3	Sector height	508cm
Sector magnet		Sector length	540cm
Number of sectors	4	Iron weight of one sector	500T
Sector angle	52°	Maximum amp. turns of auxiliary coil	4325AW
Magnet gap	10cm	Number of trim coil	36
Effective gap	6.5cm	Pole edges	Rogowski shape
Maximun field	16KG		

Radio frequency	continue
Frequency range	6.5-14MHZ
Number of Dee	2
Dee width	26°
Peak voltage	100-250KV
Rf power	120KW X 2
Harmonic number	2-10
Rough tuning($\Delta f \sim 5kc$)	Wave form moving panel
Fine tuning ($\Delta f/f < 10^{-4}$)	Inductance
Accelerating aperture	5cm
Coupling	Inductance
Q-value	7000-12000
Vacuum	
Vacuum volume of the vacuum chamber	$60m^3$
Net weight of the vacuum chamber	65T
Operating pressure	10^{-7}torr
Total gas load	$1.6X10^{-2}$ torr·l/sec
Effective pumping speed	$1.6X10^5$l/sec
10cryopumps each	ϕ 800, 20000 l/sec
Liquid nitrogen consumption	50l/hr
4 turbo molecular pumps each	3500l/sec
Buncher	
Frequency range	26-56MHZ
Harmonic number	4
Peak voltage	110KV
Number	2
SFC injector	
Number of sectors	3
Pole diameter	170.0cm
Magnet gap hill	19.0cm
valley	31.6cm
Maximum magnetic field	16KG
Flutter of the field	25-30%
Circular coils	10 pairs
Valley coils	3X3 pairs
Dee number	1
Dee angle	180°
Frequency range	6-18MHZ
Peak voltage	100KV
Rf power	300KW
Vacuum	5×10^{-6}mmHg

Table 2 Main characteristics of the accelerating system

$\frac{R_1}{R_2}$	$\frac{N_1}{N_2}$	$\frac{h_1}{h}$	f_1 (MHX)	f (MHZ)	F (Mc/s)	E (MeV/A)	η (%)
$\frac{3}{4}$	$\frac{3}{2}$	$\frac{5}{10}$	6.0-9.3	9.0-14.0	0.9-1.4	1.7-4.2	50
$\frac{3}{4}$	$\frac{3}{2}$	$\frac{3}{6}$	6.0-9.3	9.0-14.0	1.5-2.3	4.8-11.7	50
$\frac{3}{4}$	$\frac{2}{1}$	$\frac{3}{8}$	6.0-7.0	12.0-14.0	1.5-1.8	4.8-6.5	100
$\frac{3}{4}$	$\frac{1}{1}$	$\frac{3}{4}$	6.5-14.0	6.5-14.0	1.6-3.5	5.6-27.1	100
$\frac{3}{4}$	$\frac{1}{2}$	$\frac{3}{2}$	13.0-18.0	6.5-9.0	3.3-4.5	23.2-46.0	50
$\frac{3}{4}$	$\frac{3}{2}$	$\frac{1}{2}$	6.0-9.3	9.0-14.0	4.5-7.0	46.0-124.8	50

Table 3. Matching Parameters for SFC and SSC

Where h_1, f_1 ---harmonic number and radio frequency of SFC. h,f,F---harmonic number, radio frequency and orbit frequency of SSC. N_1, N_2 ---integral number. E ---extracted beam energy. $\eta (=1/N_2)$ ----matching efficiency. R_1---extraction radius of SFC. R_2---injection radius of SSC.

Sector magnet		
The stability of the magnetic field		10^{-5}
The accuracy of the isochronous field		3×10^{-4}
Field between sectors being no identify		3×10^{-4}
$(\oint \frac{\Delta B}{B} dl = 0)$		
Misalignment between sectors		
Radial translation	ΔR	$\pm$ 0.1mm
Azimuthal translation	ΔS	$\pm$ 0.1mm
Vertical translation	ΔZ	$\pm$ 0.1mm
Rotation around R axis	$\Delta\theta_R$	$\pm$ 0.30mrad
Rotation around S axis	$\Delta\theta_S$	$\pm$ 0.15mrad
Rotation around Z axis	$\Delta\theta_Z$	$\pm$ 0.03mrad
Gap error		+ 0.16mm
Sector angle error		$\pm$ 0.03mard
Rf system		
Voltage amplitude stability		10^{-3}
Phase stability		1°
Frequency stability		5×10^{-6}
Dee angle error		$\pm 0.1^{\circ}$

Table 4. Tolerances for the sector magnet and rf system

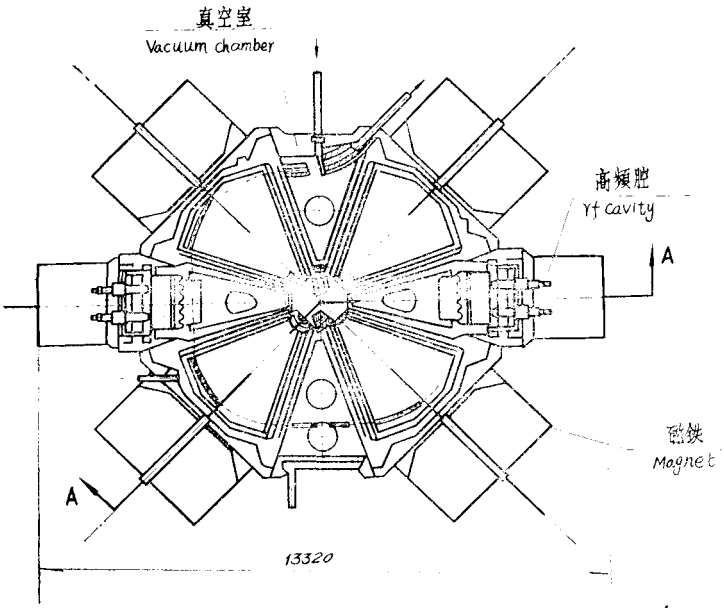

Fig.1 Schematic diagram of the main accelerator

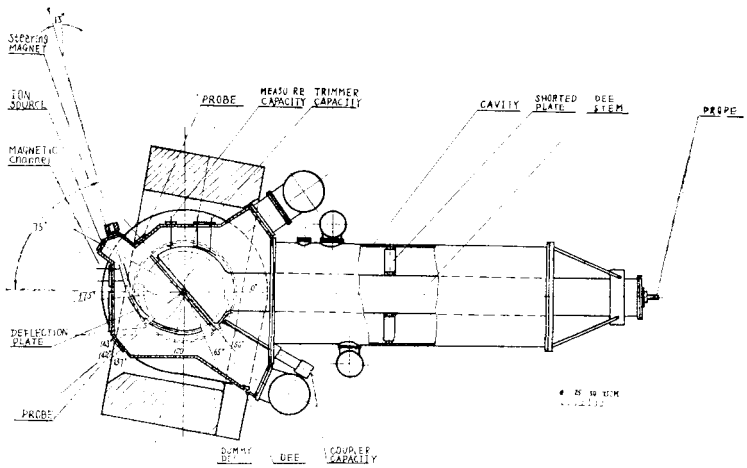

Fig.2 Schematic diagram of the injector SFC

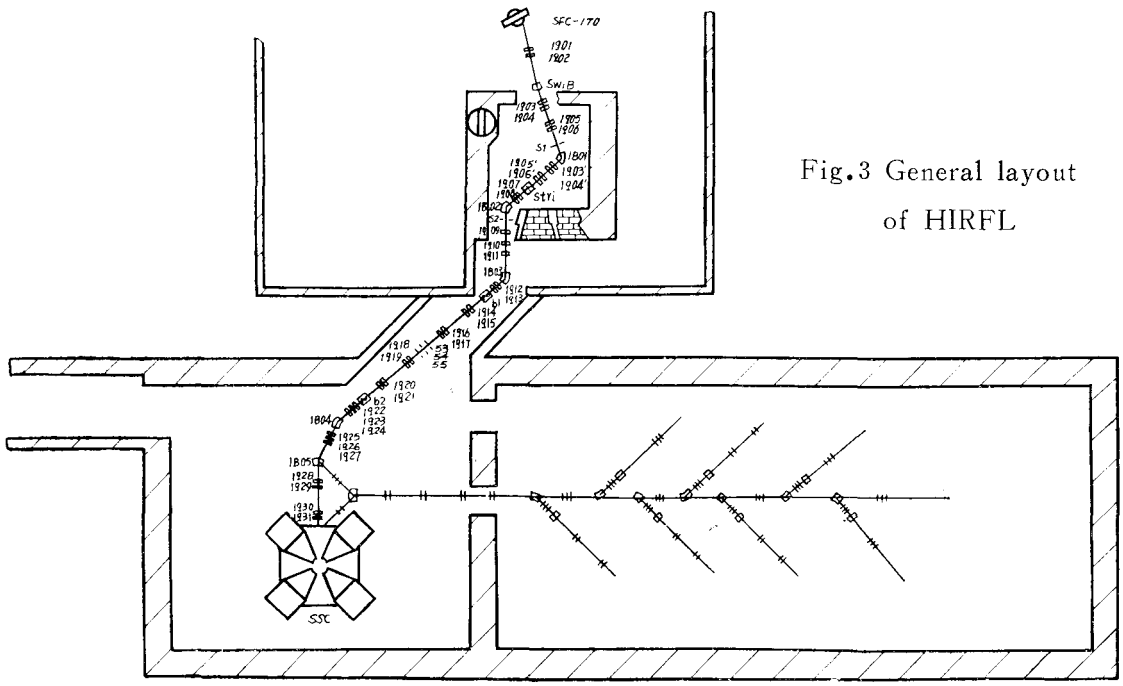

Fig.3 General layout of HIRFL

n	1	2	3	4	5	6	7	8	9	10	11
R	188.5	273.6	312.1	467.5	544.5	610.6	689.2	722.2	770.7	815.7	859.0
ΔR	84.0	84.0	103.6	80.5	67.5	58.8	52.5	47.5	43.6	40.3	40.3

mm
mm

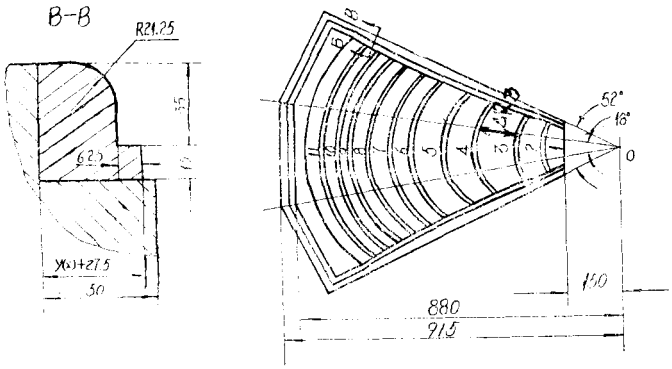

Fig.4 Pole face and edge of $\frac{1}{4}$ scale model magnet

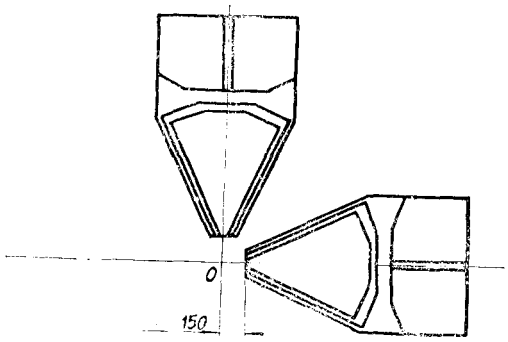

Fig.5 Arrangement of the two $\frac{1}{4}$ scale model magnets

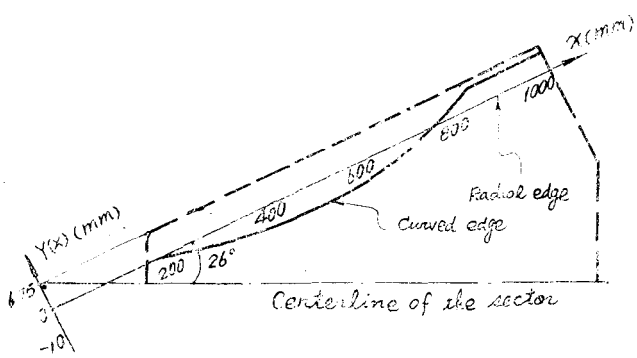

Fig.6 Curved edge of the $\frac{1}{4}$ scale model magnet

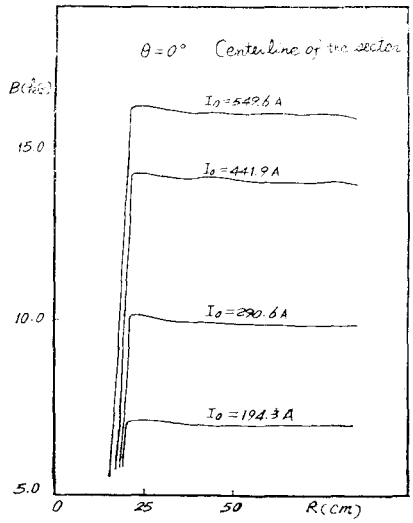

Fig.7

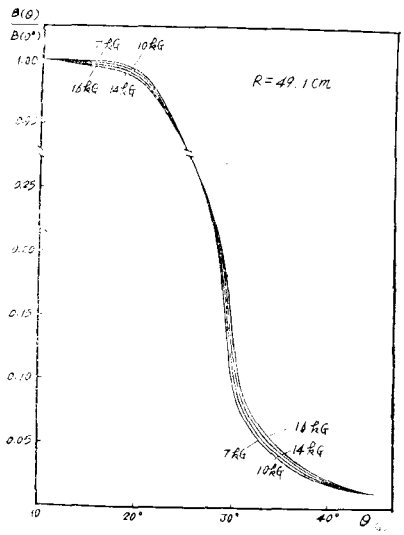

Fig.8

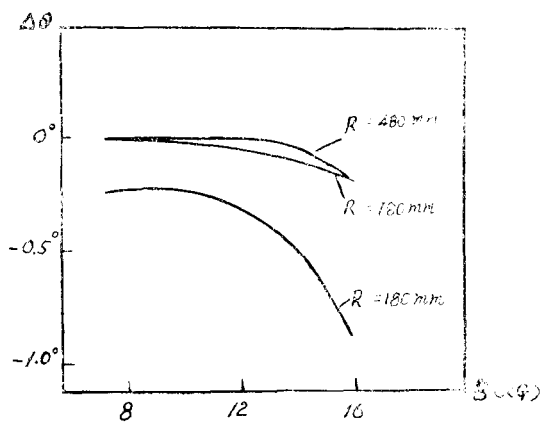

Fig.9 Magnetic angle

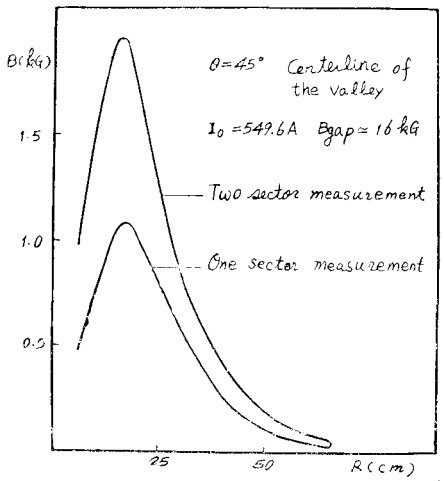

Fig.10

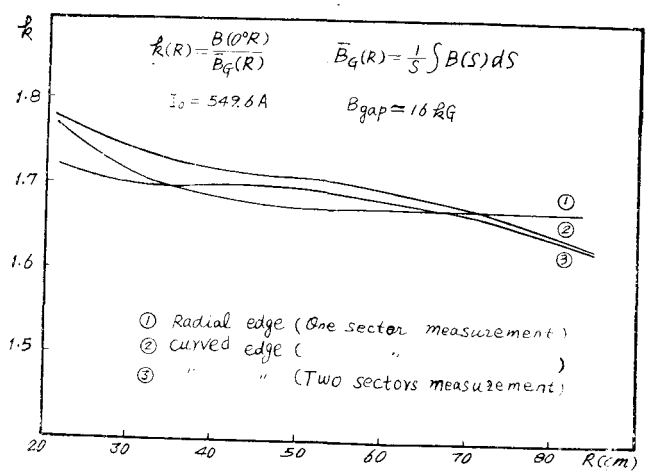

Fig.13

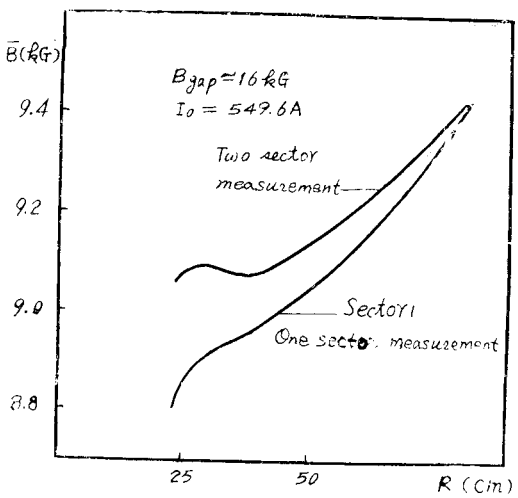

Fig.11

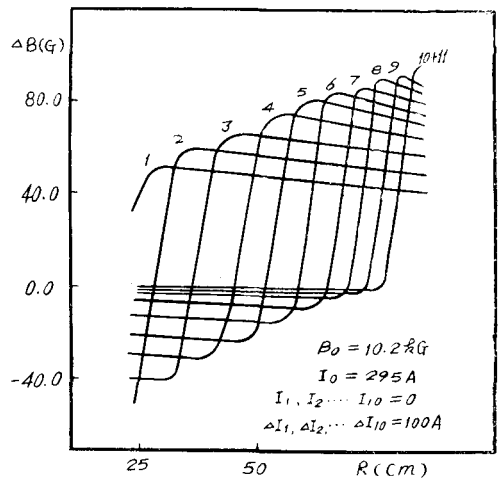

Fig.14

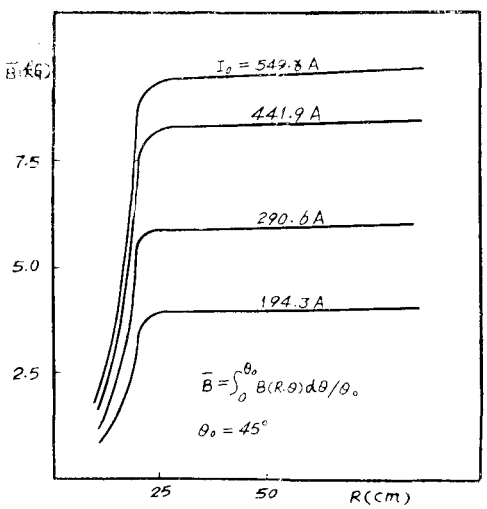

Fig.12

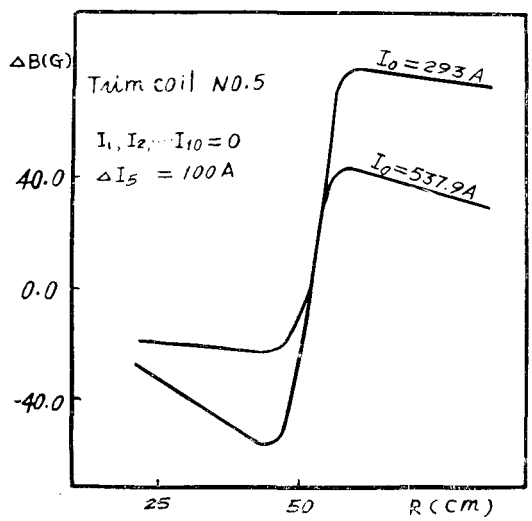

Fig.15

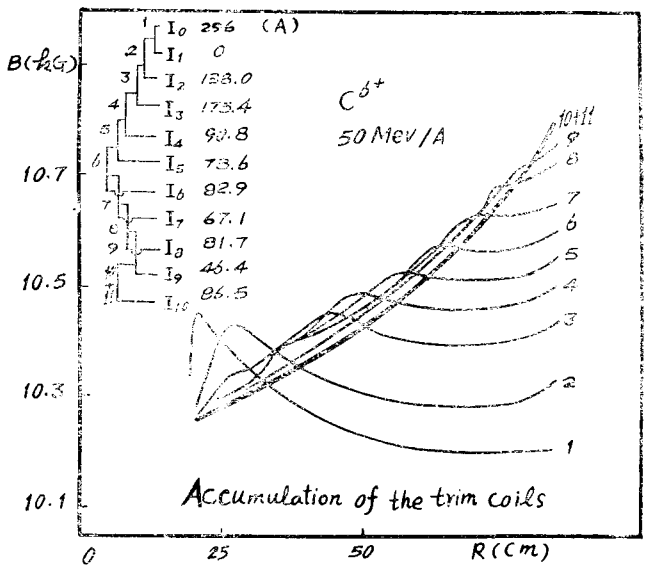

Fig.16

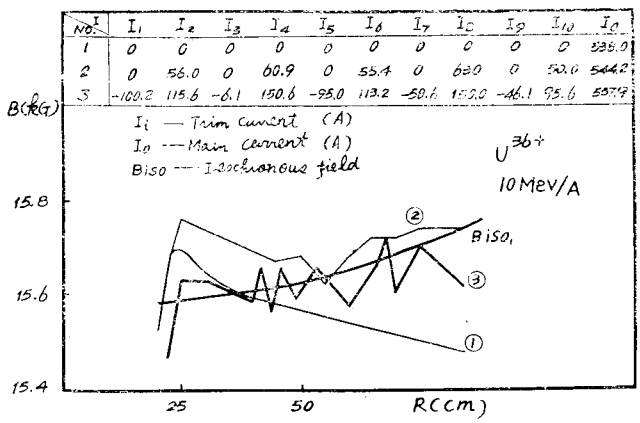

Fig.17

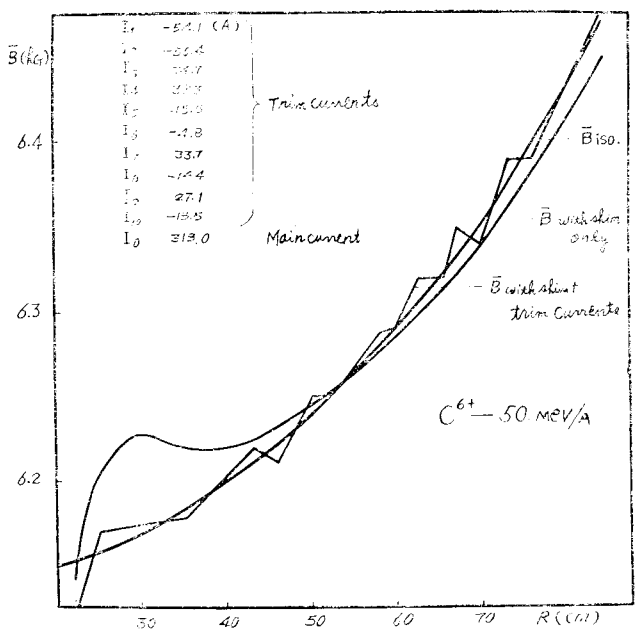

Fig.18

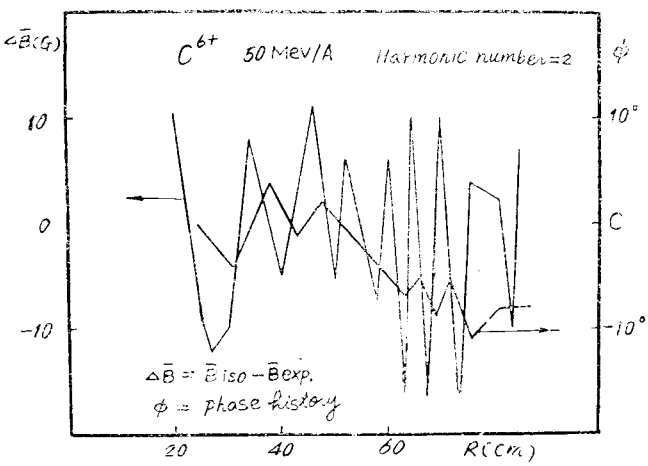

Fig.19